Generator level study of a Z' boson decaying into non-SUSY dark matter

A. Espargilière

HAL Id: in2p3-00609168

http://hal.in2p3.fr/in2p3-00609168

Submitted on 18 Jul 2011

Generator level study of a Z' boson decaying into non-SUSY dark matter

A. Espargilière

Laboratoire d'annecy-le-Vieux de Physique des Particules (LAPP), Université de Savoie, CNRS/IN2P3
e-mail: `ambroise.espargiliere@lapp.in2p3.fr`

Abstract

A Randal-Sundrum inspired model predicts a dark matter candidate together with an additional Z' boson. The detection of this boson and the measurement of its mass and production cross section at a future linear collider is investigated at the generator level. The expected accuracy of the cross section production and of the mass of the Z' boson measurements are reported.
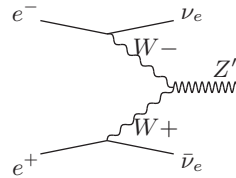
1 Introduction

Heavy Dirac neutrinos with Standard Model (SM) interactions are not viable dark matter candidates. Their large coupling to the Z^0 boson prevents them from providing the right Dark Matter (DM) relic density because of a much too high annihilation rate. This coupling would as well have made them easily detected in direct detection experiments. In the model described in [?], another type of interaction for Dirac neutrinos is proposed involving a new neutral gauge boson coupling to the right handed states, a Z' that could come from an additional $U(1)'$ or $SU(2)_R$. This Z' is suposed to have a small mixing with the SM Z^0 boson. In this model, called Right Handed Neutrino Model (RHNM), the right handed heavy Dirac neutrino, considered as a Weakly Interactive Massive Particle (WIMP) and denoted ν' in the following, becomes an interesting DM candidate because there is no coupling with the Z^0 (except through the small Z^0/Z' mixing). Therefore, with a suitable parametrisation, the model leads to the correct DM relic density and complies with the experimental direct detection constraints. The Z' may be observed at the Large Hadron Collider (LHC) [?] or at future linear colliders as studied hereafter. The Z' boson is supposed to couple mainly to the heaviest states of the SM, thus to the third SM fermion family. As top factories, the LHC and future linear colliders should be the best laboratories to discover and study those processes.

In the following, the work focuses on the Z' production in e^+e^- collisions. In the first section, a cross section study leads to the choice of the channel that will be studied at the generator level. The detailed analysis is done at a centre of mass energy of 3 TeV.
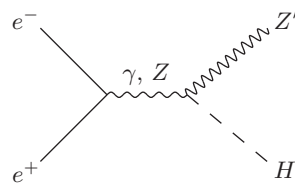
2 Cross section study

Three channels have been considered for the study of the Z' production. They are discussed below and their feynman diagrams are displayed in figure 1. Cross sections have been computed using the software calcHEP (version 2.5.5) described in [?] and references therein. The model is named: "RH_neutrino/RS-inspired". Centre of mass energy ranging from $0.5 - 3$ TeV and Z' mass ($M Z_P$) from $200\,\mathrm{GeV}/c^2$ to $3\,\mathrm{TeV}/c^2$ have been considered. The out-going Z' boson decays in heavy leptons or in WIMPs. At this step, all model parameters have been taken to arbitrary default values (couplings at 1, Z'/Z^0 mixing at 1%).

(a) $W^+ W^-$ fusion: $e^+e^- \to \nu\bar\nu Z'$

(b) "Pseudo-higgsstrahlung": $e^+e^- \to HZ'$
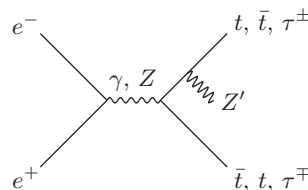
(c) Emission by an out-going fermion: $e^+e^- \to l^+l^- Z'$

Figure 1: Z' production channels

2.1 Channel $e^+e^- \to \nu\bar{\nu}Z'$

Figure 2 maps the Z' production cross section, for the complete MZ_P and centre of mass energy ranges. Some values are tabulated in table 1. The dependency of the production cross section on the Z^0/Z' mixing is linear, the values are comupted with a 1% mixing. The Z^0/Z' mixing and the Z' mass are the only non SM parameters involved in this process. The fact that the cross section keeps rising with the centre of mass energy tends to indicate a UV divergence. This hypothesis has been verified by computing the cross section at energies up to 30 TeV. The result is plotted in figure 3 and clearly confirms the UV divergence. Therefore, this effective model is not appropriate to describe this process.
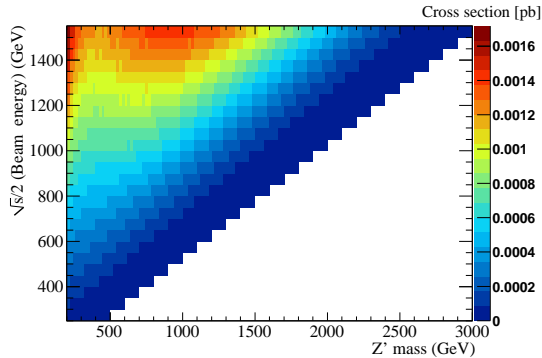

Figure 2: Map of the Z' cross section production in $W^+ W^-$ fusion process.

Table 1: Cross section of the Z' production through $W^+ W^-$ fusion.

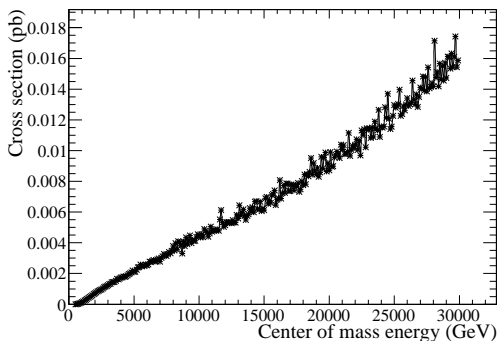| MZ_P	200	500	1000
$\sqrt{s} = 3$ TeV	1.7 fb	1.2 fb	1.4 fb
$\sqrt{s} = 1$ TeV	0.27 fb	0.14 fb	—
$\sqrt{s} = 0.5$ TeV	0.05 fb	—	—

Figure 3: Divergence of the Z' cross section production in $W^+ W^-$ fusion process in the RHNM.

2.2 Channel $e^+e^- \to HZ'$

The Higgs boson mass has been set to $120 \, \text{GeV}/c^2$. The cross section of the Z' production in this channels is mapped in figure 4 and tabulated in table 2. This process depends on the Higgs mass and Z' coupling to the Higgs boson as displayed in table 3. The dependency on the Higgs mass is not critical but constitutes an extra parameter in the study. Provided the Higgs coupling to the Z' is not too low, this channel would have a large cross sec-

tion and therefore be of great interest when results about Higgs are made available by the LHC.
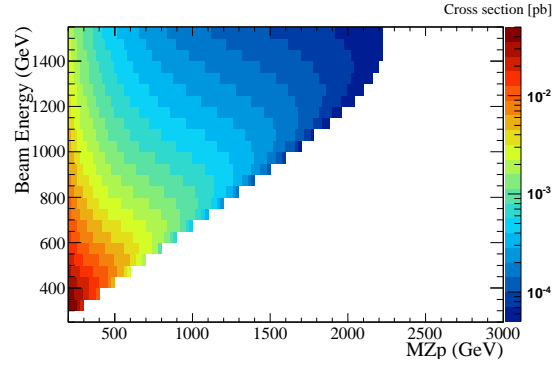

Figure 4: Map of the Z' production cross section *via* "pseudo-higgstrahlung"

Table 2: Cross section of the Z' production through "pseudo-higgstrahlung".

MZ_P	200	500	1000
$\sqrt{s} = 3$ TeV	2.2 fb	0.4 fb	0.2 fb
$\sqrt{s} = 1$ TeV	25.6 fb	8.1 fb	—
$\sqrt{s} = 0.5$ TeV	157.5 fb	—	—

Table 3: Cross section dependency on Higgs mass and Higgs coupling to the Z'.

H^0 mass	120	150	300
$gZH = 0.5$	6.4 fb	6.3 fb	5.2 fb
$gZH = 1$	25.6 fb	25.1 fb	20.8 fb
$gZH = 2$	102 fb	100 fb	83 fb

2.3 Channel $e^+e^- \to l^+l^-Z'$

Figure 5 shows the maps of the Z' production *via* emission by an out-going top quark (fig. 5(a)) or an out-going τ lepton (fig. 5(b)). Cross section values are also tabulated in table 4. The behaviour of the Z' production cross section is very similar in both cases. The difference resides in the mass of the involved fermion. The cross section maps clearly indicate that the detection of a rather light Z' (below 1 TeV) is favoured.
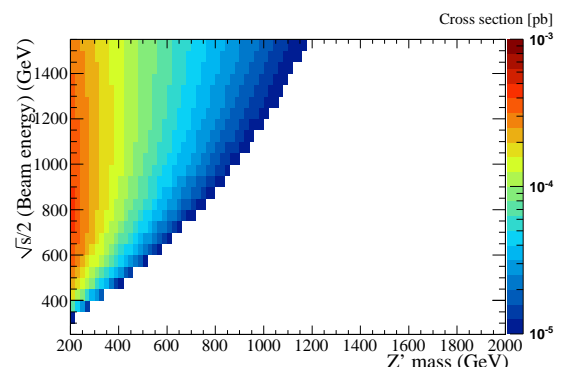
(a) case of an out-going top quark
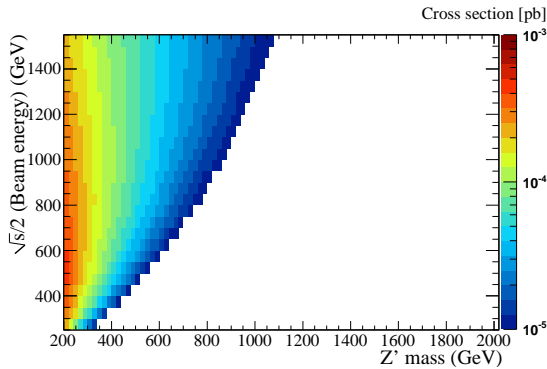
(b) case of an out-going τ lepton

Figure 5: Map of the Z' production cross section *via* emission by an out-going fermion.

Table 4: Cross section of the Z' production *via* emission by an out-going fermion.

case of the top quark			
MZ_P	200	500	1000
$\sqrt{s} = 3\,\text{TeV}$	$3.4\,\text{fb}$	$1.0\,\text{fb}$	$0.2\,\text{fb}$
$\sqrt{s} = 1\,\text{TeV}$	$3.0\,\text{fb}$	$0.04\,\text{fb}$	—
$\sqrt{s} = 0.5\,\text{TeV}$	—	—	—
case of the τ lepton			
MZ_P	200	500	1000
$\sqrt{s} = 3\,\text{TeV}$	$2.5\,\text{fb}$	$0.7\,\text{fb}$	$0.1\,\text{fb}$
$\sqrt{s} = 1\,\text{TeV}$	$4.4\,\text{fb}$	$0.2\,\text{fb}$	—
$\sqrt{s} = 0.5\,\text{TeV}$	$2.3\,\text{fb}$	—	—

2.4 Choice of the channel

The three channels considered to study the Z' production in high energy e^+e^- collisions have been discussed in the previous sections. Its production through W^+W^- fusion has been discarded because of its UV divergence. The "pseudo-higgsstrahlung" introduces extra parameters and its study should be resumed when the Higgs boson mass is known. Remains the Z' production by emission from a fermion pair. The RHNM described in [?] is very general and a fixed set of parameter values based on physical arguments is needed. In [?] a parametrisation is proposed, where the Z' boson only couples to the SM only *via* the top quark. This argument has therefore driven the choice of the channel $e^+e^- \rightarrow t\bar{t}Z'$ for a detailed analysis. The modified parameters are summarized in table 5. The mass of the ν' does not influence the Z' cross section and therefore its precise value is not critical and shall only be below $MZ_P/2$. It appears, for $MZ_P = 200\,\text{GeV/c}^2$ and $m'_\nu = 85\,\text{GeV/c}^2$, that this choice of parameter values gives the correct DM density and complies with the experimental detection limits (see annex A).

Table 5: Summary of the model parameters set to non default values

parameter name	description	value
mixzzp	Z^0/Z' mixing	0.01
gZp	Z'- ν' coupling	3
gtr	Z'- t_R coupling	3
gUp	Z'- τ coupling	0
gtl	Z-(t_L, b_L) coupling	0
gll	Z'- τ coupling	0

2.5 Choice of the decay mode

The Z' has two decay modes:

1. $Z' \rightarrow$ invisible, where "invisible" stands for the DM candidate, since the model parameter settings have suppressed the other possibilities (if one neglects the effect of the small Z^0/Z' mixing).

2. $Z' \rightarrow t\bar{t}$, leading to four-top final states.

The corresponding cross sections and branching ratios times cross section are shown in table 6.

Table 6: Total process cross sections and Z' decay branching ratios times cross section.

MZ_P	Cross sect.	$\sigma_{Z'\rightarrow\text{inv.}}$	$\sigma_{Z'\rightarrow t\bar{t}}$
$200\,\text{GeV/c}^2$	$14.9\,\text{fb}$	$14.9\,\text{fb}$	0
$300\,\text{GeV/c}^2$	$8.7\,\text{fb}$	$8.7\,\text{fb}$	0
$400\,\text{GeV/c}^2$	$5.6\,\text{fb}$	$2.4\,\text{fb}$	$3.2\,\text{fb}$
$500\,\text{GeV/c}^2$	$3.7\,\text{fb}$	$1.2\,\text{fb}$	$2.5\,\text{fb}$
$600\,\text{GeV/c}^2$	$2.6\,\text{fb}$	$0.8\,\text{fb}$	$1.8\,\text{fb}$
$700\,\text{GeV/c}^2$	$1.8\,\text{fb}$	$0.5\,\text{fb}$	$1.3\,\text{fb}$

The SM cross section for four-top events in e^+e^- collision at $3\,\text{TeV}$ is $\approx 20\,\text{ab}$, thus, provided the four top events can be correctly tagged and reconstructed, this channel will have almost no background. In addition, as the DM candidate has been taken with a mass below $MZ_P/2$, the decay of the Z' into $\nu'\bar{\nu}'$ will be always allowed. Therefore for MZ_P below $2 \times m_{\text{top}}$, invisible decay channel will be the only available. In the following the study focuses on the invisible decay of the Z'.

3 Event selection

The main characteristics of signal and backgrounds are summarised below. A method to discriminate the signal events is proposed.

3.1 Signal

The signal consists of multi-jet events with a large number of particles and a certain amount of missing energy. It is expected to be very close to SM s-channel $t\bar{t}$ events which constitute the main background. The cross sections for different mass of the Z' are shown in table 6.

3.2 Background

The signal is extracted from a sample of events tagged as $t\bar{t}$ events. In a first step, the tagging of the top events is assumed to have a full efficiency and purity. Therefore, the backgrounds considered for this study are only the SM inclusive $t\bar{t}$ events and the following background channels are leftover:

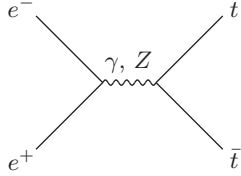$$e^+e^- \rightarrow W^+W^- \ (576\,\text{fb})$$
$$e^+e^- \rightarrow Z^0Z^0 \ (32\,\text{fb})$$
$$e^+e^- \rightarrow W^+W^-Z^0 \ (33\,\text{fb})$$
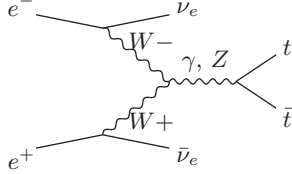$$e^+e^- \rightarrow Z^0Z^0Z^0 \ (<1\,\text{fb})$$

The present results shall then be scaled according to the real top tagging performance.

Both s and t channels $t\bar{t}$ production are considered, their respective Feynman diagrams are displayed below.

3

1. background 1: $e^+e^- \to t\bar{t}$

2. background 2: $e^+e^- \to t\bar{t} + \nu\bar{\nu}$

Their respective cross sections are summed up in table 7.

Table 7: background channel cross sections.

Channel	Cross sect.
$e^+e^- \to t\bar{t}$	19.87 fb
$e^+e^- \to t\bar{t} + \nu\bar{\nu}$	5 fb

3.3 Event generation

The program calcHEP has been used to simulate the e^+e^- collisions and generate the interaction out-going particles. The information has been stored in the "Les Houches Event" (LHE) format and fed to a Pythia8 instance [?, ?] which propagates and decays the particles.

The statistics generated correspond to the integrated luminosity of $1\,\mathrm{ab}^{-1}$, *i.e.*: about three years of operation at a luminosity of $\approx 10^{34}\,\mathrm{cm}^{-2}\,\mathrm{s}^{-1}$. In this study, the initial state energy spread takes into account the Initial State Radiation (ISR) only.

3.4 Discriminating variables

The final state variables listed in annex E are evaluated for each channel and their values are stored in a ROOT tree [?]. To give an intuitive idea of which variables are the most discriminating, the superimposition of the final state variables for the signal and the two backgrounds together with their correlations are displayed in annex D in the form of a correlation matrix with the variable spectra on the diagonal cells. Such a view lead to the conclusion that no direct cut on the variables would lead to a satisfactory separation between the signal and the two backgrounds. Some attempts not reported here have been made to apply slanted cuts in the correlation planes of the variables. This increase in complexity called for the use of Multi-Variate Analysis (MVA) tools. The Toolkit for Multi-Variate Analysis (TMVA) framework [?, ?] offers many functionalities which will be used all along this study.

Background as well as signal events are basically $t\bar{t}$ events. It is rather obvious that variables like jet masses, or the number of visible particles (or any particle counter from annex C) will not discriminate between signal and background. The differ-

ence rather lies in the event dynamics, shape and variables related to missing energy. The final variable set retained for performing the event selection is shown in the table of annex E and superimpositions of their spectrum for the signal and he two background channels, are displayed in annex H.

3.5 Classifier training and testing

A Boosted Decision Tree (BDT) has been trained separately on the two backgrounds. The input variables spectra are displayed in annex H.1 for background 1, and in H.2 for background 2. The training and testing have been done on 2×4500 events of each type. The BDT settings are shown in table 8 and the performance of the training are given in table 9. The Receiver Operating Characteristic (ROC) integral is a good indicator of the classifier's performance but, in the present case, the most important aspect is the discriminating power of the classifier when cutting at the maximum significance. Table 9 shows that in our case the classifier gives good performance compared to a simple cut on the most discriminating variable. The significance is given by:

$$S \;=\; \frac{\epsilon\,N_{\text{signal}}}{\sqrt{\epsilon\,N_{\text{signal}} + B\,N_{\text{bg.}}}}\,,$$

where ϵ is the signal efficiency at the given cut, N_{signal} is the total number of event signal, B is the background efficiency and $N_{\text{bg.}}$ the total number of background events.

Table 8: BDT parameters

|	
Boost type	Adaptative
Number of trees	1000
Maximum depth	20
Prune method	Cost complexity
Prune strength	90

Table 9: BDT performance. $\int$ ROC stands for the ROC curve integral, S_{max} denotes the maximal significance, ϵ is the signal efficiency and B is the background efficiency.

	BDT-BG1 cut Sig. *vs* Bg1	BDT-BG2 cut Sig. *vs* Bg2
$\int$ ROC	0.955	0.971
S_{max}	99.6	113.8
cut @S_{max}	-0.0378	-0.3391
ϵ@S_{max}	90.8%	97.4%
B@S_{max}	18.0%	14.6%

The BDT output for both discrimination steps are shown in figures 6(a) and 6(b) for signal *vs.* background 1 and signal *vs.* background 2 respectively. The outputs computed with the training event sample are superimposed to those computed with the testing one. A small difference between the two spectra is noticeable and is reflected by the low Kolmogorov-Smirnov probability. This indicates a slight over-training of the algorithm. A higher prune strength can avoid this (a value of 95 instead of 90 is sufficient here) but at the price of lower separation even on the test sample. Therefore, it has been considered reasonable to bear this slight over-training. The global efficiency of the event selection is 0.884 ± 0.004.
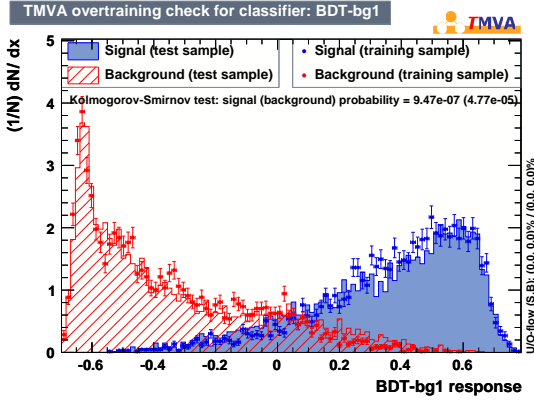
(a)
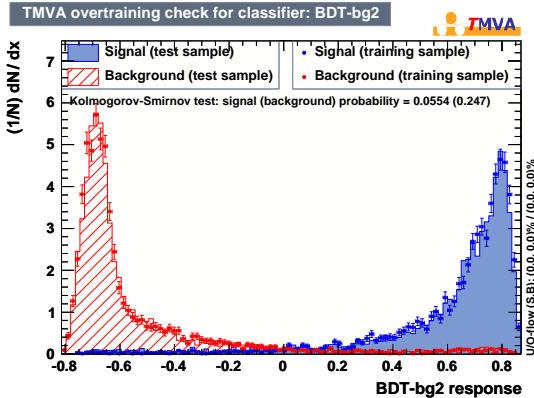
(b)

Figure 6: Response of BDT trained for bg1 rejection (6(a)) and for bg2 rejection (6(b)).

In the next section, the trained MVA methods are used to apply the two successive cuts given in table 9 on the different event samples to select the event sample from which the Z' production cross section and mass is to be measured.

4 Measurements

4.1 Method

The mass of the Z' is measured using the event invariant mass spectrum obtained after the event selection described above. Given that the Z' decays to invisible and tend to be emitted at rest or very low energy, the event total invariant mass spectrum should show a sharp upper edge corresponding to the value of the nominal centre of mass energy of $3\,\mathrm{TeV}/c^2$ minus the mass of the Z'. Nevertheless, the ISR induces a smearing of the event total invariant mass spectrum and then a smoothing of the spectrum upper edge. A function, called "smooth gate" in the following, defined in eq. 1, is fitted to the event total invariant mass spectrum without presence of the signal. This way the background contribution is modelized and is subtracted from the total spectrum. The area of the remaining spectrum is then proportional to the cross section of the $e^+e^- \to t\bar{t}Z'$ process. To measure the Z' mass, the "smooth gate" is fitted to this spectrum and the s_2 parameter, corresponding to the upper slope inflexion point, is related to $\mathrm{MZ_P}$ through the relation 4 established in section 4.2.2. The "smooth gate" is

defined by:

$$f(x) \;=\; \frac{A}{\left(e^{\frac{s_1-x}{p_1}}+1\right)\left(e^{\frac{x-s_2}{p_2}}+1\right)}, \qquad (1)$$

where s_i, $i \in \{1,2\}$ are the inflection point abscissae and p_i, $i \in \{1,2\}$ are the slope steepnesses, see graphical representation with arbitrary values of the parameters in figure 7.
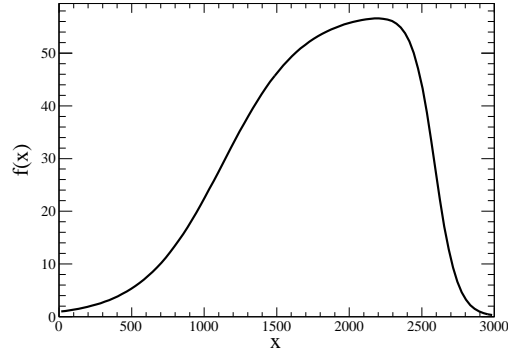

Figure 7: Smooth gate function with arbitrary parameter values.

After event selection, the cross section is calculated subtracting the background and correcting for event selection efficiency and then dividing by the $1\,\mathrm{ab}^{-1}$ luminosity.

4.2 Results

The analysis process is detailed in the next section for $\mathrm{MZ_P} = 200\,\mathrm{GeV}/c^2$. Then, in section 4.2.2, this analysis is repeated for several values of $\mathrm{MZ_P}$ and its measurement is described. Finally, in section 4.2.3, the resolution on the Z' mass is estimated.

4.2.1 Details for $\mathrm{MZ_P} = 200\,\mathrm{GeV}/c^2$

All events from the two backgrounds (20000 and 5000 for background 1 and 2 respectively) and the signal (15000) are tested with the two BDT cuts. The cut for background 2 rejection is applied first. The event invariant mass spectrum is plotted with the remaining events and displayed in figure 8. The contributions from the different sources are represented with different colours. The second background has almost vanished and the signal represents a clear excess with respect to the SM background.
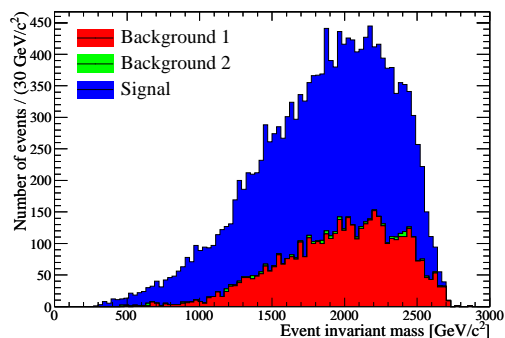

Figure 8: Event total invariant mass spectrum for signal and both backgrounds ($\mathrm{MZ_P}$ = 200 GeV/c^2).

The background contribution alone is plotted in figure 9 and the "smooth gate" function is fitted to it. The fit results are displayed in figure 9 and summarized in table 10. The total histogram (corresponding to the addition of the three contributions of the stack histogram from figure 8) is corrected by removing from each bin the value returned by the fitted "smooth gate" function evaluated at the bin centre abscissa. The corrected histogram is displayed in figure 10 and the "smooth gate" is fitted to it. The corresponding fit results are displayed on the picture and summarized in table 11.
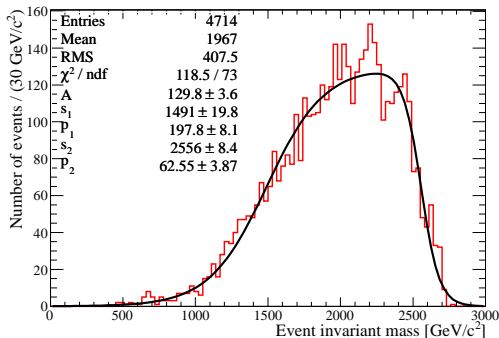

Figure 9: Event total invariant mass spectrum after event selection, for background only, fitted with the "smooth gate" function.

Table 10: Fit results for background contribution

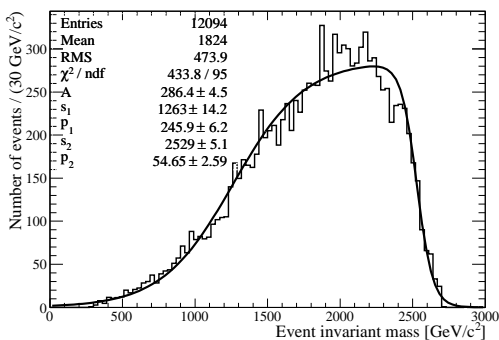|	
χ^2/ndf	118.5/73
A	129.8 ± 3.6
s_1	1491 ± 19.8
p_1	197.8 ± 8.1
s_2	2556 ± 8.4
p_2	62.6 ± 3.9

Figure 10: Event total invariant mass spectrum after event selection and background subtraction fitted with the "smooth gate" function for $MZ_P = 200 \, \mathrm{GeV}/c^2$.

Table 11: Fit results for the corrected event invariant mass spectrum.

χ^2/ndf	118.5/73
A	286.4 ± 4.5
s_1	1263 ± 15
p_1	245.9 ± 6.2
s_2	2529 ± 5.1
p_2	54.7 ± 2.6

It may be not obvious at first glance how the Z' mass can be read from those fit parameters, but remember that s_i, $i \in \{1, 2\}$ are the inflexion point abscissae. With no smearing at all the upper limit of the spectrum would show a steep end-point at $3 \, \mathrm{TeV} - MZ_P$. This corresponds to the limit when p_2 goes to 0. Then p_2 can be considered as an indicator of the smearing strength. In the same view, s_2 would match $E_{CM} - MZ_P$ in the low smearing limit. Therefore, there should be a set of parameters relating s_2 to MZ_P as:

$$s_2 = k - \alpha MZ_P, \qquad (2)$$

where k and α are parameters to determine.

In the next section, the same procedure has been repeated for various values of MZ_P to determine the values of the parameters of eq. 2.

4.2.2 Sensitivity to MZ_P

The procedure described in the previous section is applied for MZ_P from 200 to $700 \, \mathrm{GeV}/c^2$ with a constant statistics. The use of a constant statistics is meant to probe the s_2 sensitivity to MZ_P only. The resulting event invariant mass spectra are displayed in figure 11. Their fitted "smooth gate" upper inflexion point abscissa are summed up in table 12 and plotted in figure 12. This figure shows as well how a straight line is fitted to the data point and the residuals are shown in the figure corner histogram. The fit information allows to set values to the parameters in eq. 2 which now reads:

$$s_2 = (2757 \pm 8) - (1.05 \pm 0.02) \times MZ_P, \quad (3)$$

which gives a direct formula for MZ_P:

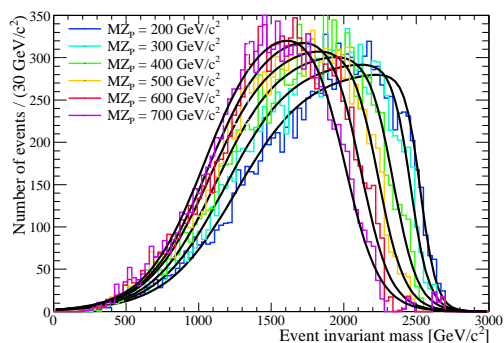$$MZ_P = \frac{(2757 \pm 8) - s_2}{1.05 \pm 0.02}. \qquad (4)$$

Figure 11: Event invariant mass spectra for various Z' masses.

Table 12: Summary of the "smooth gate" upper inflexion point abscissae (s_2)

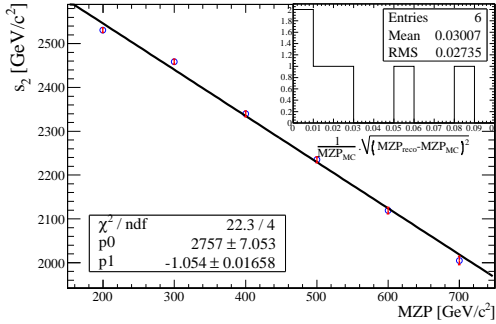| MZ_P	s_2
200	2530 ± 5.4
300	2458 ± 5.6
400	2340 ± 6.6
500	2235 ± 6.7
600	2119 ± 7.5
700	2005 ± 9.4

6

Figure 12: s_2 parameter *versus* MZ$_P$.

4.2.3 Resolution on MZ$_P$

Thanks to eq. 4, it is now possible to predict the Z' mass from a $t\bar{t}$ event invariant mass spectrum to which a "smooth gate" function is fitted (see definition in eq. 1). As $MZ_P = (k - s_2)/\alpha$, the error margin on this prediction reads:

$$\Delta MZ_P = \underbrace{\frac{\Delta k}{\alpha}}_{\substack{\text{constant} \\ \text{term}}} \oplus \underbrace{\frac{MZ_P \Delta \alpha}{\alpha}}_{\substack{\text{linear} \\ \text{term}}} \oplus \underbrace{\frac{\Delta s_2}{\alpha}}_{\substack{\text{fit} \\ \text{term}}} \quad (5)$$

$$= 7.8\,\text{GeV}/c^2 \oplus 0.95\Delta s_2 \oplus 1.9\%MZ_P$$

See annex G for the detailed calculation of this error.

The errors Δk and $\Delta \alpha$ are inherent to the measurement method itself. Hence, the constant and the linear term of eq. 5 describe systematic uncertainties. They may be reduced by refining the analysis on the s_2 dependency on MZ$_P$ described in the previous section (4.2.2). For instance, using more statistics for each value of MZ$_P$ and/or using more values of MZ$_P$ are possible refinements. Whereas the error Δs_2 comes from the event invariant mass spectra fitted with the "smooth gate" function and can only be improved by the accumulation of more statistics. Thus, the so-called "fit term" reflects the statistical uncertainty on MZ$_P$.

To evaluate correctly the expectable resolution on MZ$_P$, the statistics predicted by the model must be used. Table 13 sums up the main features of the analysis using the model predicted statistics: for each mass, the table shows the number of events passing the MVA cuts and surviving the background subtraction, the value of the s_2 parameter with its error and the significance of the new physics signal. It appears here that above MZ$_P$ $=500\,\text{GeV}/c^2$ the event yield is not sufficient to perform a reliable fit and the s_2 returned values do not make sense any more, thus the Z' mass would not be measurable. Nevertheless, given that the SM predicts about 4700 events passing the cuts, the Z' discovery may still be allowed in virtue of the obtained significance, the measured cross sections are shown in table 14. The present method tend to underestimate the process cross section for low MZ$_P$ and slightly over-estimate it at higher values.

Table 13: Z' events using model predicted statistics

MZ$_P$	events yield	s_2	significance
200	12094	2529 ± 5.1	92.7
300	7411	2448 ± 7.7	66.6
400	2150	2342 ± 19.7	24.6
500	1192	2282 ± 39.5	13.5
600	815	913 ± 82	8.4
700	642	962 ± 78	5.6

Table 14: Z' cross section measurement result

MZ$_P$	True cross sect.	Measured cross sect.
200	14.9 fb	13.7 fb
300	8.7 fb	8.4 fb
400	2.4 fb	2.4 fb
500	1.2 fb	1.3 fb
600	0.8 fb	0.9 fb
700	0.5 fb	0.7 fb

For MZ$_P$ between 200 and 500 GeV/c^2 a resolution is predicted using eq. 5 and values from table 13. The result is plotted in figure 13.
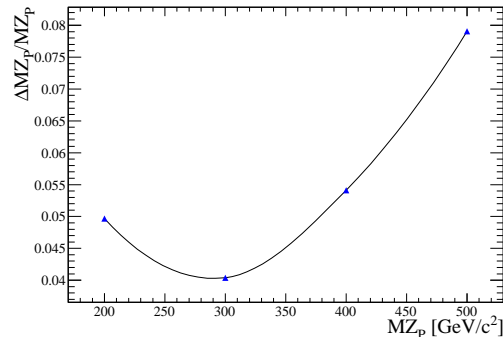

Figure 13: MZ$_P$ error *vs.* MZ$_P$.

5 Conclusion

A generator level analysis of the predictions of a Randall-Sundrum-inspired model furnishing right handed neutrino as a dark matter candidate coupling to an additional gauge boson Z' (either $SU(2)_R$ or $U(1)'$) has been carried out. The study focused on the $e^+e^- \to t\bar{t}Z'$ channel, with the Z' decaying into WIMPs. A method to measure the Z' mass has been proposed. If the Z' has a mass below $500\,\text{GeV}/c^2$, it may be measured with a precision better than 10% with $1\,\text{ab}^{-1}$ of data, and therefore may guide a threshold energy scan to reach better resolution. Shall the Z' mass be around $600\,\text{GeV}/c^2$ or higher, a discovery would still be possible but no mass estimation could be cast. The results given here are subject to review when a full simulation or at least a realistic smearing of the MVA input variables is available.

Acknowledgements

like especially to thank Jean-Jacques Blaising for advices, useful discussions and precious help.

Contents

References

[1] Geneviève Bélanger, Alexander Pukhov, and Géraldine Servant. Dirac neutrino dark matter. *Journal of Cosmology and Astroparticle Physics*, january 2008. doi: 10.1088/1475-7516/2008/01/009.

[2] Alexander Pukhov. Calchep 2.3: Mssm, structure functions, event generation, batchs, and generation of matrix elements for other packages. *arXiv:hep-ph/0412191*, 2004.

[3] C.B. Jackson, Géraldine Servant, Gabe Shaughnessy, Tim M.P. Tait, and Marco Taoso. Higgs in space! *Journal of Cosmology and Astroparticle Physics*, 2010(04):004, 2010.

[4] Pythia 8 home page. http://home.thep.lu.se/~torbjorn/Pythia.html.

[5] Torbjörn Sjöstrand. Introduction to pythia8. Talk at Nordic Workshop on LHC and Beyond, June 2008. http://home.thep.lu.se/~torbjorn/talks/nordita08.pdf.

[6] ROOT home page. http://root.cern.ch.

[7] A. Hoecker, P. Speckmayer, J. Stelzer, J. Therhaag, E. von Toerne, and H. Voss. *TMVA 4 User Guide*, arxiv:physics/0703039 edition, November 2007. http://tmva.sourceforge.net/docu/TMVAUsersGuide.pdf.

[8] TMVA home page. https://twiki.cern.ch/twiki/bin/view/TMVA/WebHome.

A   Dark matter relic density and detection rate

The DM relic density and the direct detection event rate are calculated using micrOMEGAS2.2, with $MZ_P = 200\,\text{GeV}/c^2$ and $m_{\nu'} = 85\,\text{GeV}/c^2$.

$$\Omega_{\nu'} = 0.11$$

WIMP-nucleon spin independent scattering cross section:

$$\sigma_{\nu'-p} = 5.8 \cdot 10^{-9}$$
$$\sigma_{\nu'-n} = 5.3 \cdot 10^{-7}$$

Direct detection event rate for ^{73}Ge and ^{131}Xe targets:

$$^{73}\text{Ge:}\ 0.058\ /\text{day/kg}$$
$$^{131}\text{Xe:}\ 0.12\ /\text{day/kg}$$

B   Summary of the cross sections and statistics for the signal.

MZ_P (GeV/c^2)	Cross sect.	Width($Z' \to$ inv.)	Width($Z' \to t\bar{t}$)	Br($Z' \to$ inv.)	$Z' \to$ inv.
200	14.9 fb	19.4 GeV	0 GeV	100%	15000
300	8.7 fb	32.8 GeV	0 GeV	100%	8700
400	5.6 fb	45.5 GeV	60.3 GeV	43.0%	2408
500	3.7 fb	57.9 GeV	115.0 GeV	33.0%	1240
600	2.6 fb	70.1 GeV	162.0 GeV	30.2%	785
700	1.8 fb	82.3 GeV	205.5 GeV	28.6%	515

C   Index of the final state variables

Variable name	Description	Range
ttM	$t\bar{t}$ system invariant mass	0–3000 GeV/c^2
evtM	Event invariant mass	0–3000 GeV/c^2
missE	Missing energy	0–3000 GeV
missP	Missing momentum	0–3000 GeV/c
missA	Cosine of polar angle of missing momentum	-1–1
missPT	Missing transverse momentum	0–3000 GeV/c
missM	Missing mass	0–3000 GeV/c^2
sphericity	Event sphericity	0–1
aplanarity	Event aplanarity	0–0.5
jet1P	First jet momentum	0–3000 GeV/c
jet1PT	First jet transverse momentum	0–3000 GeV/c
jet1E	First jet energy	0–3000 GeV
jet1M	First jet mass	0–3000 GeV/c^2
jet2P	Second jet momentum	0–3000 GeV/c
jet2PT	Second jet transverse momentum	0–3000 GeV/c
jet2E	Second jet energy	0–3000 GeV
jet2M	Second jet mass	0–3000 GeV/c^2
nPart	Number of particles	$\in \mathcal{N}$
nTrack	Number of charged particles	$\in \mathcal{N}$
nHadr	Number of hadrons	$\in \mathcal{N}$
nHadrC	Number of charged hadrons	$\in \mathcal{N}$
nGamma	Number of photons	$\in \mathcal{N}$
nElect	Number of electrons	$\in \mathcal{N}$
nMu	Number of muons	$\in \mathcal{N}$

D   Final state correlation matrix
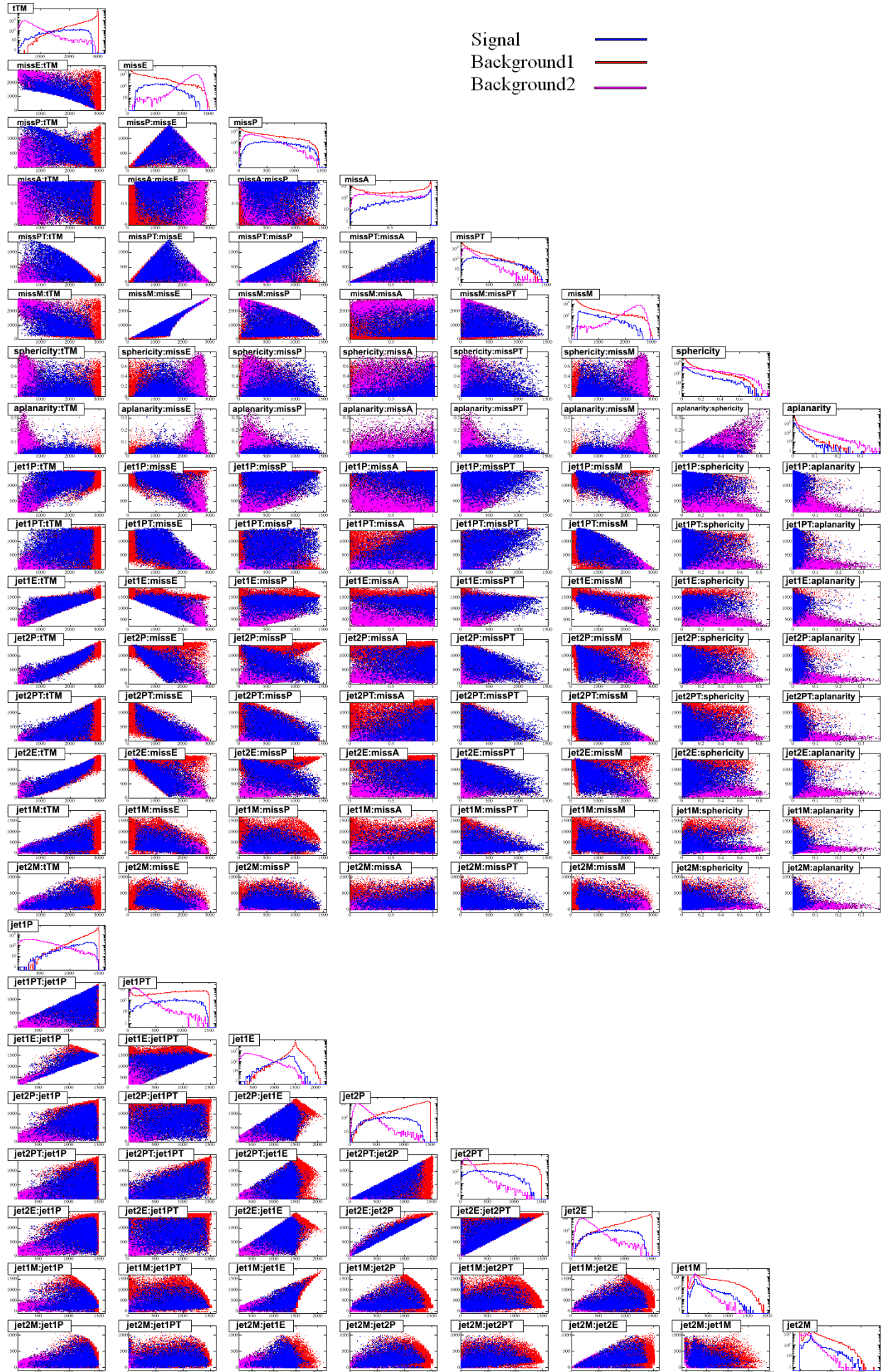
E Summary of the analysis variables

Variable name	Description	Discriminating power
`missPT`	Missing transverse momentum	3.462e-01
`missE`	Missing energy	3.114e-01
`jet1E`	First jet energy	3.012e-01
`jet2E`	Second jet energy	2.496e-01
`jet2P`	Second jet momentum	2.365e-01
`missP`	Missing momentum	2.250e-01
`jet1P`	First jet momentum	2.138e-01
`jetPTdiff:=jet1P-jet2P`	jet PT diffrence	2.122e-01
`missA`	Angle of missing momentum	1.134e-01
`jet2PT`	Second jet transverse momentum	1.078e-01
`sphericity`	Sphericity	1.024e-01
`aplanarity`	Aplanarity	9.443e-02
`jetEratio:=jet2E/jet1E`	Jets energy ratio	9.302e-02
`Jet1PT`	First jet transverse momentum	7.763e-02
`jetEdiff:=jet1E-jet2E`	Jets energy difference	6.089e-02

F BDT variable importance ranking

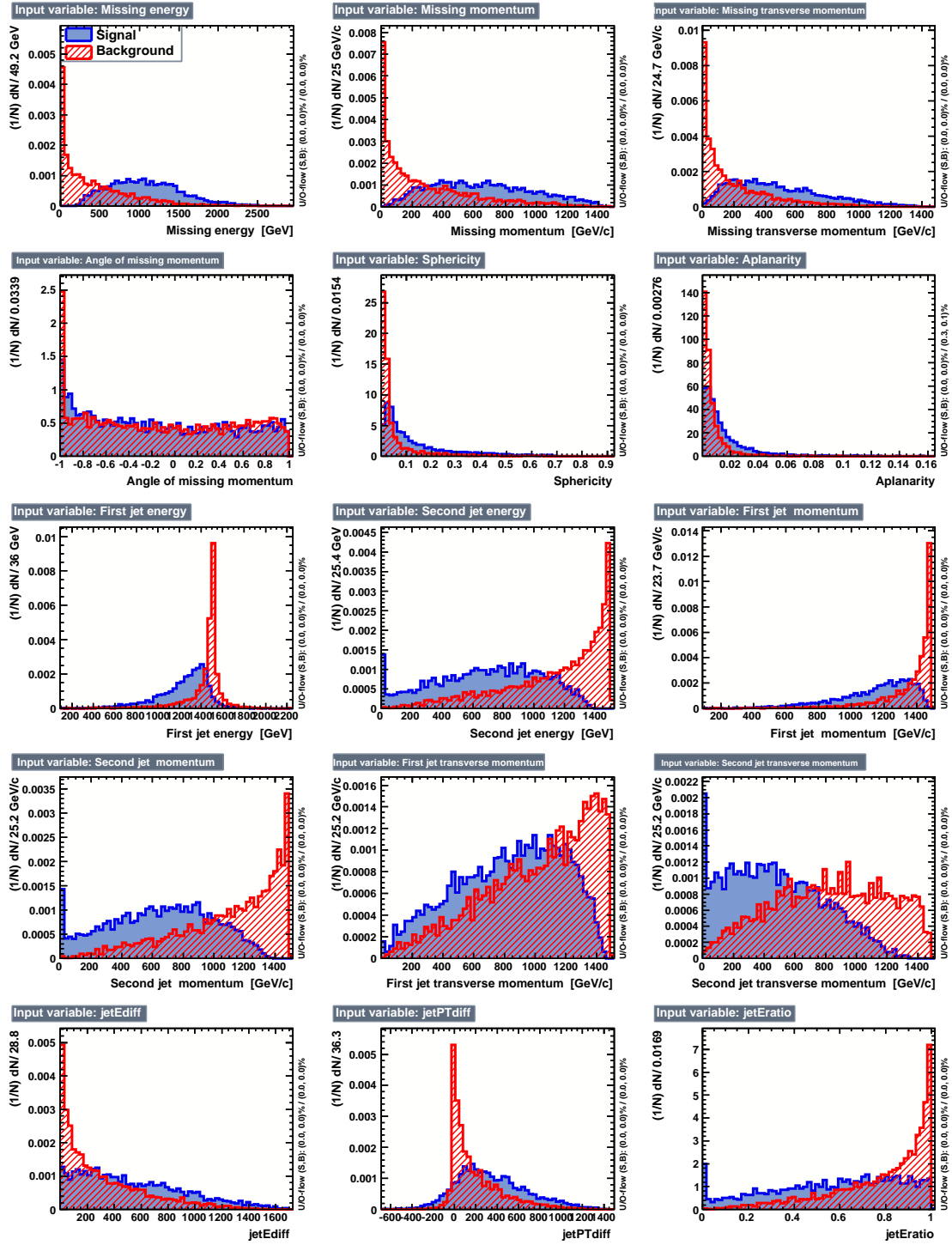| Rank	Variable	Importance
1	missPT	1.929e-01
2	missE	1.366e-01
3	jet1P	1.069e-01
4	jet1E	8.365e-02
5	jet1PT	6.978e-02
6	missA	5.944e-02
7	missP	5.346e-02
8	jet2E	4.576e-02
9	jetEratio	4.288e-02
10	jetPTdiff	4.001e-02
11	jet2PT	3.919e-02
12	jet2P	3.636e-02
13	sphericity	3.534e-02
14	jetEdiff	2.973e-02
15	aplanarity	2.799e-02

G $\mathrm{MZ_P}$ measurement error calculation.

As described in section 4.2.2, the Z' mass relates to the upper inflection point abscissa of the "smooth gate" fitted on the event invariant mass spectrum, denoted s_2. The error is derived from this relation:

$$\mathrm{MZ_P}(s_2) = \frac{k - s_2}{\alpha}$$

$$\Rightarrow \frac{\Delta^2 \mathrm{MZ_P}}{(\mathrm{MZ_P})^2} = \frac{\Delta^2(k - s_2)}{(k - s_2)^2} + \frac{\Delta^2\alpha}{\alpha^2} \qquad \text{with } \Delta^2(k - s_2) = \Delta^2 k + \Delta^2 s_2$$

$$\Rightarrow \frac{\Delta^2 \mathrm{MZ_P}}{(\mathrm{MZ_P})^2} = \frac{\Delta^2 k}{(k - s_2)^2} + \frac{\Delta^2 s_2}{(k - s_2)^2} + \frac{\Delta^2\alpha}{\alpha^2} \qquad \text{but } (k - s_2)^2 = \alpha^2 (\mathrm{MZ_P})^2$$

$$\Rightarrow \Delta^2 \mathrm{MZ_P} = \frac{\Delta^2 k}{\alpha^2} + \frac{\Delta^2 s_2}{\alpha^2} + \frac{\mathrm{MZ_P}\Delta^2\alpha}{\alpha^2}$$

$$\Rightarrow \Delta \mathrm{MZ_P} = \sqrt{\frac{\Delta^2 k}{\alpha^2} + \frac{\Delta^2 s_2}{\alpha^2} + \frac{\mathrm{MZ_P}\Delta^2\alpha}{\alpha^2}} \qquad \text{which also reads :}$$

$$\Delta \mathrm{MZ_P} = \frac{\Delta k}{\alpha} \oplus \frac{\Delta s_2}{\alpha} \oplus \frac{\mathrm{MZ_P}\Delta\alpha}{\alpha}$$

H MVA input variable spectrum

H.1 Signal versus background 1

H.2   Signal versus background 2